

The Impact of Non-Gaussianity upon Cosmological Forecasts

A. Repp¹, I. Szapudi¹, J. Carron^{1,2}, and M. Wolk¹

¹*Institute for Astronomy, 2680 Woodlawn Dr., Honolulu, Hawaii 96822, USA*

²*Department of Physics and Astronomy, University of Sussex, Brighton BN1 9QH, U.K.*

14 February 2022

ABSTRACT

The primary science driver for 3D galaxy surveys is their potential to constrain cosmological parameters. Forecasts of these surveys’ effectiveness typically assume Gaussian statistics for the underlying matter density, despite the fact that the actual distribution is decidedly non-Gaussian. To quantify the effect of this assumption, we employ an analytic expression for the power spectrum covariance matrix to calculate the Fisher information for BAO-type model surveys. We find that for typical number densities, at $k_{\max} = 0.5h \text{ Mpc}^{-1}$, Gaussian assumptions significantly overestimate the information on all parameters considered, in some cases by up to an order of magnitude. However, after marginalizing over a six-parameter set, the form of the covariance matrix (dictated by N -body simulations) causes the majority of the effect to shift to the “amplitude-like” parameters, leaving the others virtually unaffected. We find that Gaussian assumptions at such wavenumbers can underestimate the dark energy parameter errors by well over 50 per cent, producing dark energy figures of merit almost 3 times too large. Thus, for 3D galaxy surveys probing the non-linear regime, proper consideration of non-Gaussian effects is essential.

Key words: surveys – cosmological parameters – cosmology: theory

1 INTRODUCTION

Cosmological surveys provide the primary data set for characterizing the universe as a whole. It was surveys of the cosmic microwave background (CMB) which revealed the small anisotropies (Smoot et al. 1992; Bennett et al. 2013; Planck Collaboration et al. 2014) presumed to be the progenitors of today’s large scale structure; and a primary goal of recent galaxy surveys is to constrain the parameters of the Λ -Cold Dark Matter (Λ CDM) model (e.g., Tegmark et al. 2004 for the Sloan Digital Sky Survey and Cole et al. 2005 for the Two-degree Field Galaxy Redshift Survey). The term “precision cosmology” reflects the resulting increased knowledge of these parameter values.

Inflationary theories typically predict the high degree of Gaussianity displayed by the CMB (e.g., Bardeen et al. 1986; Bond & Efstathiou 1987). Given that the universe’s matter distribution arose from the fluctuations visible in the CMB, the galaxy power spectrum constitutes a powerful summary statistic for much of the information in galaxy surveys (e.g., Peebles 1980; Baumgart & Fry 1991; Martínez 2009).

Future widefield surveys will attempt to ascertain more precisely the galaxy power spectrum and thus the dark energy equation of state (Blake et al. 2011; Mellier 2012). The planning of such surveys depends heavily on forecasting tools, which calculate the degree to which the survey will constrain the parameters of interest. The primary such tool is the Fisher information matrix (Fisher 1925), first applied to cosmology by Jungman et al. (1996a; 1996b), by Vogeley & Szalay (1996), and by Tegmark et al. (1997). Calculating the Fisher matrix requires one to assume a particular form for the galaxy power spectrum covariance (see Section 2); thus it also necessitates an understanding of the distribution of the underlying field. One typically assumes this field to be Gaussian (e.g., Seo & Eisenstein 2007; Wang et al. 2010; Albrecht et al. 2009). For CMB fluctuations this assumption is justified. However, for galaxy surveys, the over- and underdensities are distinctly non-Gaussian, for two reasons. First, galaxies’ discrete realization of the underlying dark matter field introduces Poisson shot noise into surveys (e.g., Peebles 1980; Neyrinck et al. 2011). Second – and more problematically – gravitational amplification of the primordial fluctuations alters the original Gaussian matter field to a distinctly non-Gaussian distribution (Fry & Peebles 1978; Sharp et al. 1984; Bouchet et al. 1993; Szapudi et al. 1992; Gaztanaga 1994).

As a result of this non-linearity, the different Fourier k -modes are now correlated rather than independent (Meiksin & White 1999; Rimes & Hamilton 2005; Neyrinck et al. 2006). Hence, the power spectrum covariance matrix is no longer strictly diagonal (as in the Gaussian case) but contains off-diagonal entries described by the trispectrum rather than by the power spectrum itself. Furthermore, surveys of finite size have limited ability to resolve nearby k -modes, the resolving power being inversely proportional to the linear scale of the survey. One effect of non-linear growth is to couple these unresolved nearby Fourier modes to the large-scale beat mode between them; this is the “beat coupling” phenomenon, first described by Hamilton et al. (2006) (see also Sefusatti et al. 2006). Thus the covariance of the non-linear power spectrum is dominated by the largest scale (super-survey) modes, and an ade-

quate description of the information in the non-linear regime must account for both the intra-survey trispectrum and the coupled super-survey modes. Hence, a significant portion of the information inherent in the survey escapes from the power spectrum, causing an “information plateau” at higher values of k (Lee & Pen 2008; Carron 2011; Carron & Neyrinck 2012).

Thus the (typical) forecasting assumption of a Gaussian field leads (at high k -values) to inaccurate information estimates and therefore to inaccurate forecasts. Existing work has not thoroughly investigated the quantitative impact of this assumption. We thus present here a method for quantifying the effect which Poisson sampling of a non-Gaussian field exercises upon forecasts. Initial results show that at $k_{\max} = 0.5h \text{ Mpc}^{-1}$ it significantly influences information estimates for all parameters considered, by up to an order of magnitude for certain amplitude-like parameters.

Previous work by Takada & Jain (2009) showed for weak lensing surveys that marginalization over a parameter set can reduce the effect of non-Gaussianity on forecasting. We show (for galaxy surveys) the reason that marginalization affects certain parameters more than others. In particular, it is the amplitude-like parameters which carry the effect of non-Gaussianity after marginalization, leading in turn to a dark energy figure of merit up to 2.9 times too large. Upon publication we will make available a code which realizes our method.

The structure of this paper is as follows. In Section 2 we describe our method of calculating Fisher information. In Section 3 we compare our method to simulations. In Sections 4–6 we quantify the impact of assuming Gaussianity, and we show that this assumption results in underestimates of the dark energy parameter errors of more than 50 per cent. We discuss the effects of marginalization in Section 5, and we conclude in Section 7.

2 METHOD

The Fisher matrix quantifies the information which a random variable carries about the parameters upon which it depends. The random variable in this case is the power spectrum $P(k)$, which depends on a vector of cosmological parameters $\boldsymbol{\theta} = [\theta_1, \theta_2, \dots, \theta_n]$. If $p(P(k); \boldsymbol{\theta})$ is the probability of observing values $P(k)$ of the power spectrum given a set of parameter values $\boldsymbol{\theta}$, then the entries of the $(n \times n)$ Fisher matrix are

$$F_{ij} = \left\langle \frac{\partial \ln p(P(k); \boldsymbol{\theta})}{\partial \theta_i} \frac{\partial \ln p(P(k); \boldsymbol{\theta})}{\partial \theta_j} \right\rangle, \quad (1)$$

or equivalently

$$F_{ij} = - \left\langle \frac{\partial^2 \ln p(P(k); \boldsymbol{\theta})}{\partial \theta_i \partial \theta_j} \right\rangle. \quad (2)$$

The Cramér-Rao Inequality (Rao 1945; Cramér 1946) elucidates the importance of the Fisher matrix, stating that if \hat{D}_i is a set of unbiased estimators for observable quantities D_i , then

$$\text{Cov}(\hat{D})_{ij} \geq \sum_{\alpha, \beta} \frac{\partial D_i}{\partial \theta_\alpha} (F^{-1})_{\alpha\beta} \frac{\partial D_j}{\partial \theta_\beta}, \quad (3)$$

where $\text{Cov}(\hat{D})$ is the covariance matrix for the estimators \hat{D}_i . This inequality thus provides the link between the Fisher matrix and the (co-)variances of the observables. Two results follow. First, if the estimated quantities D_i are identical to the parameters θ_i , then the inverse Fisher matrix sets a lower bound on the possible covariance of the parameters:

$$\Sigma_{ij} \geq (F^{-1})_{ij}, \quad (4)$$

where Σ is the covariance matrix for the parameters θ_i .

Second, if we take the observables D_i to be the power spectrum values $P(k_i)$ and further require that all information be derived from these observables in the context of a physical theory, then the inequality becomes an equality, and

$$F_{\alpha\beta} = \sum_{k_i, k_j \leq k_{\max}} \left(\frac{\partial P(k_i)}{\partial \alpha} \text{Cov}_{ij}^{-1} \frac{\partial P(k_j)}{\partial \beta} \right), \quad (5)$$

where α and β are cosmological parameters of interest and where Cov_{ij} is the covariance matrix of the power spectrum modes. It is through Cov_{ij} that the non-Gaussianity of the matter field enters the calculation.

Assuming no shot noise, Equation 5 yields the following standard approximation (Tegmark 1997) for the Fisher matrix on a Gaussian field:

$$F_{\alpha\beta}^G = \frac{V}{2} \int_{k_{\min}}^{k_{\max}} dk k^2 \frac{\partial \ln P(k)}{\partial \alpha} \frac{\partial \ln P(k)}{\partial \beta}. \quad (6)$$

Here V is the volume of the survey, and k_{\min} and k_{\max} are the minimum and maximum wavenumbers under consideration. In most cases it suffices to assume that k_{\min} vanishes.

Our goal is to contrast the information $F_{\alpha\beta}^G$ in a Gaussian field with the information $F_{\alpha\beta}$ in a Poisson-sampled non-Gaussian field. Since non-Gaussianity affects the Fisher matrix through Cov_{ij} , we require an expression for the power spectrum covariance in the non-Gaussian case. Carron et al. 2015 (hereinafter CWS15) introduce the following approximation based on simulations by Neyrinck (2011b) and Mohammed & Seljak (2014):

$$\text{Cov}_{ij} = \delta_{ij} \frac{2(P(k_i) + \frac{1}{\bar{n}})^2}{N_{k_i}} + \sigma_{\min}^2 P(k_i) P(k_j), \quad (7)$$

where N_{k_i} is the number of Fourier modes in the k_i -shell in Fourier space, and where \bar{n} is the average galaxy number density.

The behavior of the Fisher information in the non-linear regime is a direct consequence of this specific form for the covariance matrix. In this expression, the first term is the Gaussian covariance, modified to include shot noise; the second term parametrizes the non-Gaussianity of the underlying field by means of σ_{\min}^2 . As CWS15 note (see discussion around their eqn. 29), one can obtain this covariance matrix by starting with a Gaussian field and then modulating it with a stochastic amplitude parameter whose variance is σ_{\min}^2 . As we note later (see Section 5 and Appendix A), the result is that the effects of non-Gaussianity appear in the amplitude-like parameters, while the other parameters retain essentially Gaussian behavior.

The quantity σ_{\min}^2 represents the minimum achievable variance for a log-amplitude parameter $\ln A_0$, defined by

$$\frac{\partial P(k_i)}{\partial \ln A_0} = P(k_i). \quad (8)$$

Note that this parameter A_0 is distinct from the initial amplitude A of the linear power spectrum. A_0 measures non-linear amplitude, and one could thus take it to equal σ_8^2 in the linear regime, in which case it would differ slightly from σ_8^2 on the translinear scales which we consider.

σ_{\min}^2 thus marks an inherent information plateau for the standard power spectrum of a non-Gaussian field. CWS15 further decompose σ_{\min}^2 into σ_{SS}^2 and σ_{IS}^2 . The first component σ_{SS}^2 expresses the impact of large-scale (super-survey) modes through beat coupling. The second component σ_{IS}^2 expresses the impact of small-scale (intra-survey) couplings on the trispectrum.

CWS15 then derive the following expression for the Fisher matrix $F_{\alpha\beta}$:

$$F_{\alpha\beta} = F_{\alpha\beta}^G - \sigma_{\min}^2 \frac{F_{\alpha \ln A_0}^G F_{\ln A_0 \beta}^G}{1 + \sigma_{\min}^2 F_{\ln A_0 \ln A_0}^G}. \quad (9)$$

To include Poisson sampling, we note that shot noise appears only in the Gaussian term of the covariance expression; thus it suffices to modify the expression for F^G (following Tegmark 1997) to read

$$F_{\alpha\beta}^G = \frac{V}{2} \int_{k_{\min}}^{k_{\max}} \frac{dk k^2}{2\pi^2} \frac{\partial \ln(P(k) + \frac{1}{n})}{\partial \alpha} \frac{\partial \ln(P(k) + \frac{1}{n})}{\partial \beta}, \quad (10)$$

with Equation 9 remaining unchanged.

The final step is to approximate σ_{\min}^2 ; we again follow CWS15. The hierarchical ansatz (Peebles 1980; Fry 1984) allows us to approximate both components analytically. We can write the intra-survey component as

$$\sigma_{\text{IS}}^2 = 8 \int_V \frac{d^3x}{V} \int_V \frac{d^3y}{V} \frac{\xi^2(x-y)}{\sigma^2}, \quad (11)$$

where ξ is the two-point correlation function and σ^2 is the variance (δ^2) of the matter field; we can further approximate Equation 11 as

$$\sigma_{\text{IS}}^2 = 8 \frac{P(k_{\max})}{V}. \quad (12)$$

Likewise, from Takada & Hu (2013) we can express the super-survey component as

$$\sigma_{\text{SS}}^2 = \left(\frac{26}{21}\right)^2 \cdot \frac{1}{2\pi^2} \int dk k^2 P_{\text{lin}}(k) W(k)^2. \quad (13)$$

In this expression, $P_{\text{lin}}(k)$ specifies the linear power spectrum, and $W(k)$ is the Fourier transform of the window function $W(x)$ (which equals $1/V$ inside the volume and vanishes outside of it). The factor of $26/21$ reflects the fact that we are defining the fluctuations δ with respect to the observed local density (as appropriate for a galaxy survey). If we were defining it with respect to a global density (e.g., for a weak lensing survey) the factor would become $68/21$. The factors differ because the local mean density includes the contribution of background modes, so that

$$\delta(x)_{\text{local}} = \frac{\delta(x)_{\text{global}}}{1 + \delta_{\text{bkgd}}}. \quad (14)$$

See table 1 of Wolk et al. (2015) for values of σ_{IS}^2 and σ_{SS}^2 at redshifts from $z = 0$ to 2. Note also that in Equations 12 and 13, $P(k)$ and $P_{\text{lin}}(k)$ refer to *unbiased* power spectra, so that σ_{\min}^2 does not depend upon the galaxy bias one assumes.

Since σ_{\min}^2 is simply the sum of σ_{IS}^2 and σ_{SS}^2 , we can now calculate the Fisher information matrix under the assumption of Poisson sampling of a non-Gaussian field.

To implement this formula, we generate (non-linear) power spectra with CAMB¹ (Cosmic Anisotropies in the Microwave Background, Lewis et al. 2000), which uses the halo fit model of Takahashi et al. (2012). From these spectra we numerically calculate partial derivatives using symmetric difference quotients ($\Delta\alpha/\alpha = 0.05$). For fiducial cosmological parameter values we use Planck 2015 (Planck Collaboration et al. 2015).

3 VALIDATION

To validate this procedure, we attempted to reproduce the error-bar results of Neyrinck 2011a (hereinafter N11). N11 bases his calculations on the 37 cosmological simulations composing the Coyote Universe suite (Heitmann et al. 2010, 2009; Lawrence et al. 2010). He obtains an ensemble of power spectra for each cosmology, and from these power spectra he estimates the covariance. Since we use Equation 7 to approximate the covariance, comparison of our results with these simulations will both validate our method in general and further establish the accuracy of this approximation.

Equation 5 shows that calculation of Fisher information requires not only the covariance but also the derivatives of the power spectrum. N11 estimates these derivatives directly from the variations in the realizations of the Coyote Universe cosmologies. These cosmologies specify parameters $\Omega_m h^2$, $\Omega_b h^2$, n_s , w , and σ_8 , from which they calculate the Hubble constant parameter h (based on the angular scale of the CMB acoustic peaks, Lawrence et al. 2010).

We must however consider two subtleties. First, such a procedure makes h a function of the other five parameters rather than an independent variable. This fact mandates some care if we are to reproduce N11's partial derivatives. If α is the vector of the five parameter values, then

$$P(k) = P(\alpha, h(\alpha), k); \quad (15)$$

thus a derivative calculated from the Coyote Universe simulations involves an extra term due to the implicit α -dependence of h :

$$\left(\frac{\partial P}{\partial \alpha}\right)_{\text{CU}} = \frac{\partial P}{\partial \alpha} + \frac{\partial P}{\partial h} \frac{\partial h}{\partial \alpha}. \quad (16)$$

We therefore must estimate $\partial h / \partial \alpha_i$ for given values of α . To do so, we employ the parameter values from table 1 of Lawrence et al. (2010); we form a simplex from the six points closest to α in 5-dimensional parameter space; and we determine ∂h by interpolation on that simplex.

The second subtlety concerns the fact that it suffices for N11 to model $\partial P(k) / \partial \alpha$ in terms of fluctuations away from the mean power spectrum of the 37 cosmologies. This procedure yields one derivative for the Coyote Universe suite as a whole, whereas our method calculates a separate $\partial P(k) / \partial \alpha$ for each cosmology. Thus we must compare N11's one error bar (for each parameter) to our ensemble of 37 error bars (for each parameter).

We hence calculate Fisher information (and thus error bars) as functions of k_{\max} for each of the 37 Coyote Universe cosmologies, and we display the results in Fig. 1. The blue line in each panel denotes the mean error bar over the 37-member ensemble, and the green shading indicates the 1-sigma range of the error bars (again over the suite of 37 cosmologies). The corresponding curves in N11 are those plotted in black along the diagonal of his fig. 7. Comparison at $k_{\max} = 0.1 \text{ Mpc}^{-1}$ shows that, with one exception, our results agree with those of N11 to within 1σ (where σ here is the standard deviation of the error bar sizes over the Coyote Universe ensemble). At $k_{\max} = 0.5 \text{ Mpc}^{-1}$ the results agree (again with one exception) to within 1.5σ . The exception in both cases is $\ln \sigma_8^2$, where N11's results differ from ours by 1.5σ and 2.4σ at $k = 0.1$ and 0.5 Mpc^{-1} , respectively. However, even in this more nearly discrepant case, the error bars we obtain for $\ln \sigma_8^2$ in the non-Gaussian case are on average *lower* than those which N11 obtain from simulations. Thus N11's simulations show that the effect of non-Gaussianity on σ_8 will be at least as large as stated in this work – and possibly larger. Hence we conclude that our method, based on the CWS15 approximation, yields results comparable to cosmological simulations.

¹ <http://camb.info/>

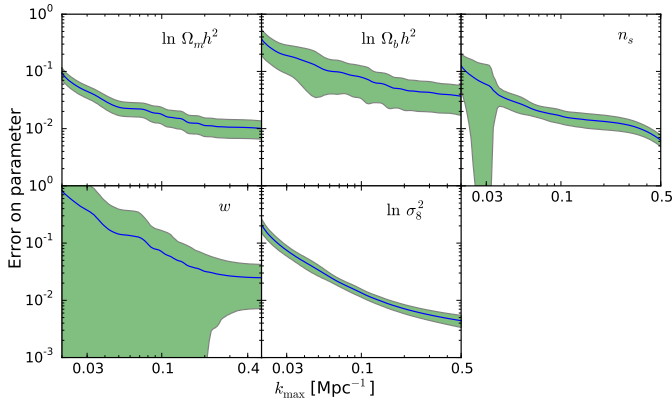


Figure 1. Size of (unmarginalized) error bars for the five Coyote Universe parameters. The blue line in each panel denotes the mean over the 37 Coyote Universe cosmologies, and the green shaded regions mark the range of $1\text{-}\sigma$ variation over those cosmologies. Comparison with fig. 7 of N11 demonstrates that our results agree with the N11 simulation-based results within 1σ for $k_{\text{max}} = 0.1 \text{ Mpc}^{-1}$ and within 1.5σ for $k_{\text{max}} = 0.5 \text{ Mpc}^{-1}$, with one exception in both cases. The exception is $\ln \sigma_8^2$, which differs from N11’s results by 1.5σ in the first case and 2.4σ in the second (see text for discussion). We conclude that our method returns results comparable to those obtained from simulations.

For the remainder of this paper we fix $h = 0.6774$ (the Planck 2015 value) for our calculations, and we quote results in terms of h (e.g., units of k are $h \text{ Mpc}^{-1}$).

4 RESULTS: FISHER INFORMATION

We can now compare the Fisher information on various parameters, under different covariance assumptions (Gaussian vs. non-Gaussian), and under different sampling assumptions (continuous vs. Poisson). We here consider the following six parameters: $\Omega_c h^2$ and $\Omega_b h^2$ (the physical cold dark matter and baryon densities, respectively); n_s (the spectral index for the primordial power spectrum); w and w_a (the dark energy equation of state and its derivative); and σ_8 (the linear amplitude parameter). We simulate three 1-Gpc^3 surveys, at $z = 0, 0.5$, and 1 ; and we assume a galaxy bias of unity. We consider two mean galaxy number densities throughout. The first is $\bar{n} = 0.003 h^3 \text{ Mpc}^{-3}$, which corresponds roughly (Hu & Haiman 2003) to the Sloan Digital Sky Survey (SDSS) Main Galaxy Sample (MGS). The second is $\bar{n} = 0.0003 h^3 \text{ Mpc}^{-3}$, which corresponds roughly (Anderson et al. 2012) to the Baryon Oscillation Spectroscopic Survey (BOSS). For comparison we also consider the limiting case of a continuous field.

We first calculate the absolute Fisher information for each parameter. As an example, Fig. 2 shows the information in the survey at $z = 0.5$ (chosen since this redshift represents a regime of transition from matter domination to dark energy domination). One notes that the different covariance assumptions typically begin to affect the results even before $k_{\text{max}} = 0.1 h \text{ Mpc}^{-1}$, although the details vary from parameter to parameter.

Since our purpose is to quantify the impact of non-Gaussianity, it is more instructive to consider the ratio (Gaussian to non-Gaussian) of information rather than the absolute amount of information. Thus we display these ratios in Fig. 3 for each parameter, for each redshift, and for each sampling assumption. In general the effects increase with wavenumber, as expected given the information plateau described in Sections 1 and 2.

Table 1. Error ratios, non-Gaussian to Gaussian

$k_{\text{max}} [h \text{ Mpc}^{-1}]$	Ratios of Error Bar Sizes					
	$\Omega_c h^2$	$\Omega_b h^2$	n_s	w	w_a	σ_8
0.1	1.00	1.00	1.00	1.28	1.30	1.04
$\bar{n} = 0.003$	1.00	1.00	1.00	1.25	1.27	1.03
$\bar{n} = 0.0003$	1.00	1.00	1.00	1.11	1.11	1.02
0.2	1.01	1.00	1.00	1.71	1.81	1.30
$\bar{n} = 0.003$	1.00	1.00	1.00	1.56	1.62	1.24
$\bar{n} = 0.0003$	1.00	1.00	1.00	1.15	1.15	1.07
0.5	1.01	1.04	1.15	2.80	2.78	3.87
$\bar{n} = 0.003$	1.01	1.04	1.17	2.34	2.30	2.88
$\bar{n} = 0.0003$	1.01	1.01	1.05	1.26	1.21	1.33

Ratio of error bar sizes under non-Gaussian assumptions to those under Gaussian assumptions. Calculations assume the combination of three hypothetical 1-Gpc^3 surveys at $z = 0, 0.5$, and 1 . For each maximum wavenumber the first row displays the limiting case of a continuous matter distribution, while the second and third rows assume Poisson sampling with $\bar{n} = 0.003$ and $0.0003 h^3 \text{ Mpc}^{-3}$ respectively (representative of the SDSS MGS and BOSS samples). We assume a galaxy bias of unity.

The magnitude of the effect is clearly non-negligible, especially for the dark energy parameters and for σ_8 . Consider for instance a 1-Gpc^3 survey similar to the SDSS MGS, and assume that the survey considers wavenumbers up to $k = 0.5 h \text{ Mpc}^{-1}$. The lower left panel of Fig. 3 shows that assuming Gaussian covariance at $z = 0$ will lead one to predict an information content for w more than 9 times greater than in the real (non-Gaussian) universe. Since Fisher information scales as volume, the 1-Gpc^3 survey will thus yield only the information expected from a 0.1-Gpc^3 survey. In other words, Gaussian assumptions can cause an order of magnitude overestimate of Fisher information.

For smaller number densities the effect can still be significant: reference to the lower right panel of Fig. 3 shows that forecasts of information on σ_8 for a BOSS-type 1-Gpc^3 survey at $z = 0$ are three times greater under Gaussian assumptions than under non-Gaussian at $k_{\text{max}} = 0.5 h \text{ Mpc}^{-1}$. Thus, while it is safe to assume Gaussian statistics in the linear regime, doing so at higher wavenumbers can drastically inflate the predicted information content. Future surveys such as Euclid aim to probe this non-linear region on scales approaching $1 h \text{ Mpc}^{-1}$ (Hearin et al. 2012). Thus, though the effect is subtle for linear wavenumbers, the effect will be profound for future surveys, as we demonstrate in the next two sections.

5 MARGINALIZATION

Fisher analysis in this context is a tool to forecast confidence limits for future surveys. Thus we must translate these information ratios into error bar sizes. In calculating unmarginalized errors for a single parameter, one assumes perfect knowledge of the remainder of the parameter set; thus one considers only the diagonal elements of the Fisher matrix. So in the unmarginalized case, the minimum standard deviation for the i th parameter is

$$\sigma_i = 1/\sqrt{F_{ii}} \quad (17)$$

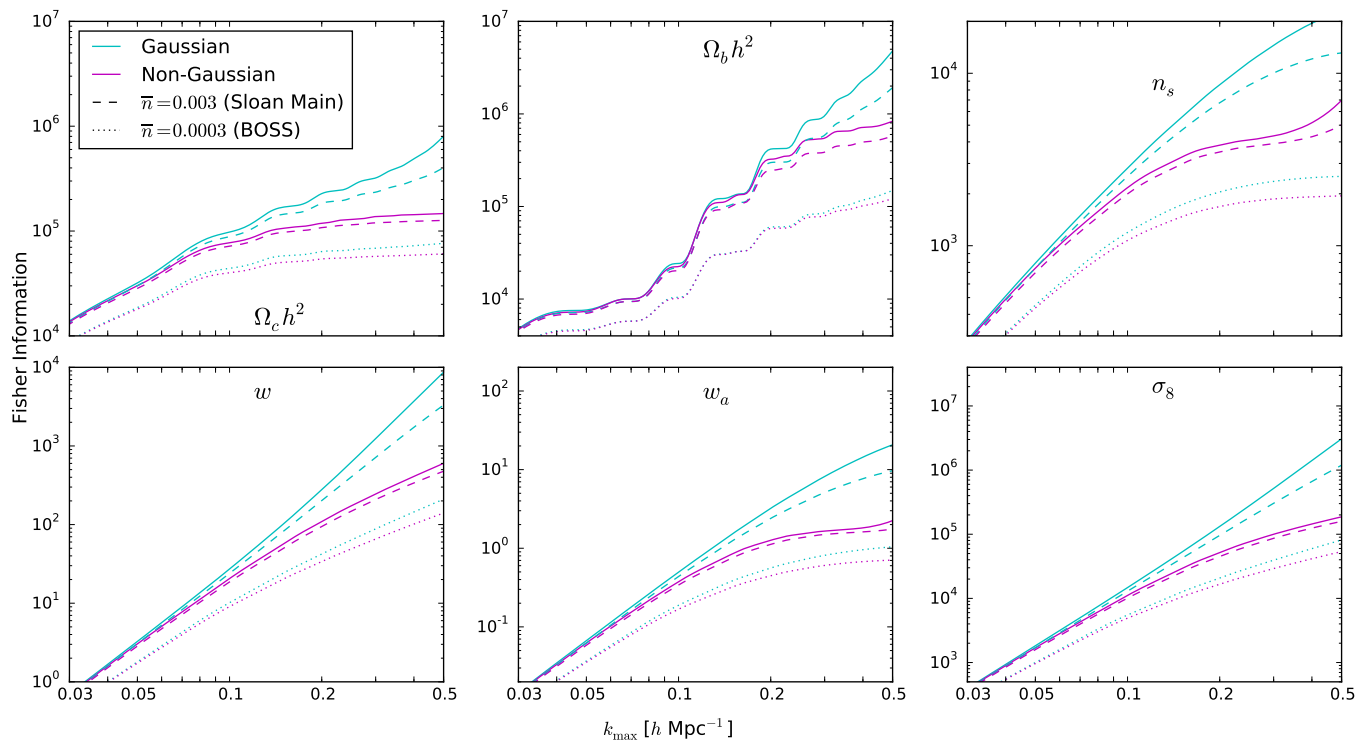


Figure 2. Fisher information under both Gaussian and non-Gaussian assumptions for a hypothetical 1-Gpc³ survey at $z = 0.5$. Solid curves represent the limiting case of a continuous matter field; dashed and dotted curves assume Poisson sampling with $\bar{n} = 0.003$ and $0.0003 h^3 \text{ Mpc}^{-3}$ respectively (comparable to the SDSS MGS and to the BOSS sample). We use Equation 9 to calculate the information for non-Gaussian cases. Note that the scale of the vertical axis differs from panel to panel. We assume a galaxy bias of unity.

by Equation 4. Inspection of Fig. 3 shows that the ratio of unmarginalized error bars can be greater than 3 for parameters like σ_8 .

More useful for our purposes, however, are the error bars derived from marginalizing over the possible values of the remaining parameters. In this case one must invert the entire Fisher matrix to obtain the matrix of parameter covariances (Equation 4). We show in Appendix A that if the amplitude parameter $\ln A_0$ (defined by Equation 8) is part of the parameter set, and if the Fisher matrix is invertible, then the entire effect of non-Gaussianity appears in the error bars for $\ln A_0$; perhaps surprisingly, non-Gaussianity has no effect on the remaining parameters. This result is a direct consequence of the form of the power spectrum covariance matrix derived from simulations and expressed in Equation 7.

However, there are two caveats to this result. First, it depends on the invertibility of the Gaussian Fisher matrix and otherwise fails. Furthermore, as F^G approaches singularity, the matrix becomes increasingly ill-conditioned and thus numerically unstable with respect to inversion. In such a case one is attempting to analyse too many parameters simultaneously. One solution is to shrink the parameter set; another is to impose a prior; a third is to obtain more data to break the degeneracy (for instance, by combining data from multiple redshifts).

The second caveat is that no standard cosmological parameter is strictly equal to $\ln A_0$; thus one cannot in practice expect all non-Gaussian effects to accumulate in one parameter. However, one does expect “amplitude-like” parameters (such as σ_8 and the dark energy parameters w and w_a) to be the ones which particularly exhibit the effects of non-Gaussianity.

Thus, if $\ln A_0$ is part of the parameter set, marginalization

concentrates the entire effect of the non-Gaussianity into the error bars for that one parameter; but if $\ln A_0$ is not part of the parameter set, marginalization distributes these effects among the amplitude-like parameters. Takada & Jain (2009) showed that marginalization can reduce the impact of non-Gaussianity; what our analysis demonstrates is the mechanism by which it does so. In particular, it is the form of the power spectrum covariance matrix which pushes the effects from the other parameters into the amplitude-like parameters.

6 RESULTS: PARAMETER ERRORS

In calculating the ratios of marginalized error bars for our model surveys, we noted an information degeneracy of σ_8 with w . We reduce this degeneracy by combining the results from our three hypothetical 1-Gpc³ surveys (redshifts 0, 0.5, and 1) to take advantage of the increasing importance of dark energy at low redshifts. The error bar ratios (for the same parameters and number densities as before) appear in Fig. 4 and in Table 1.

As predicted, non-Gaussianity has virtually no effect on the matter density parameters, whereas the effect is pronounced for the amplitude-like parameters w , w_a , and σ_8 . For these parameters, the error bars in SDSS MGS-type surveys (at high wavenumbers) can be more than double that predicted by Gaussian forecasting; even for BOSS-type samples, the error bars can exceed Gaussian predictions by over 30 per cent.

Focusing specifically on w and w_a , Fig. 5 and Table 2 demonstrate the impact of non-Gaussianity on the Dark Energy Task Force

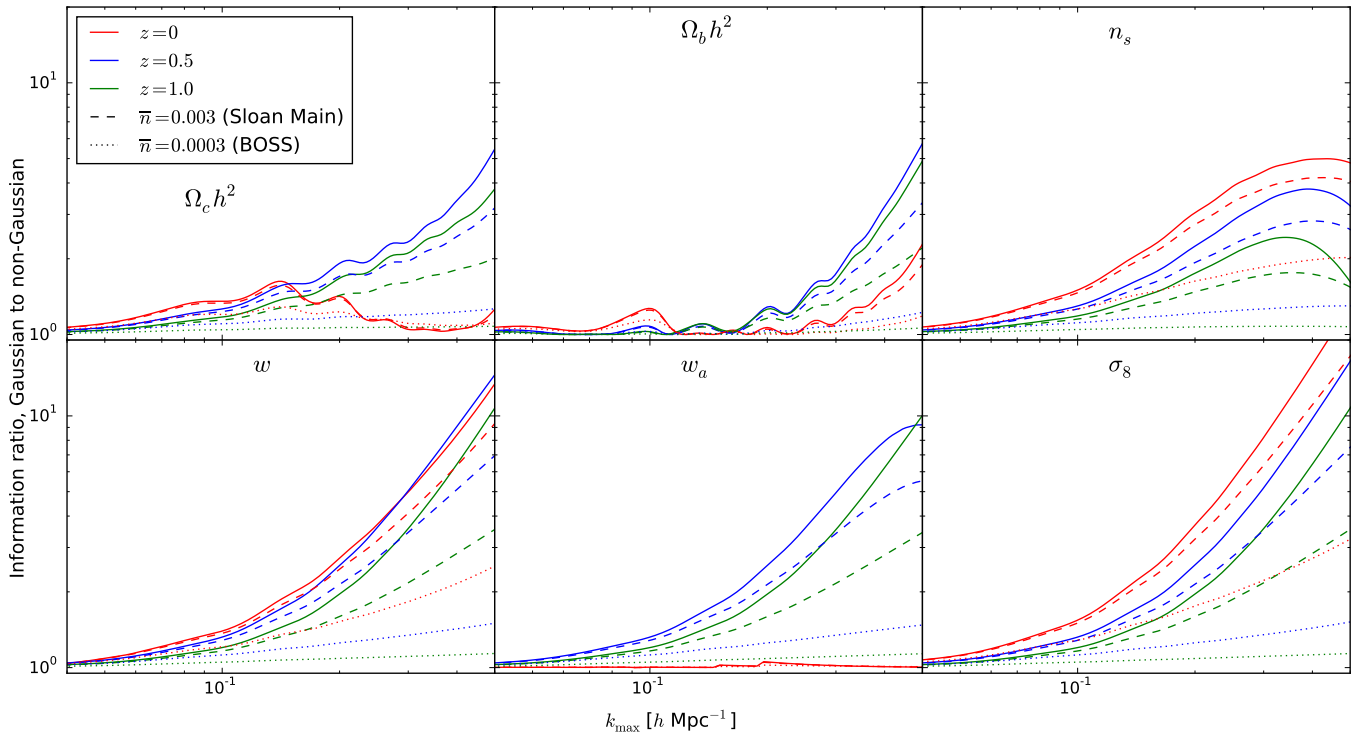


Figure 3. Ratio of Fisher information under Gaussian assumptions to that under non-Gaussian assumptions, for three hypothetical 1-Gpc³ surveys at $z = 0, 0.5,$ and 1 . Solid curves represent the limiting case of a continuous matter field; dashed and dotted curves assume Poisson sampling with $\bar{n} = 0.003$ and $0.0003 h^3 \text{ Mpc}^{-3}$ respectively (comparable to the SDSS MGS and to the BOSS sample). We use Equation 9 to calculate the information for non-Gaussian cases. Note that for typical number densities, the assumption of Gaussian covariance can cause an order of magnitude overestimate for the information content on certain parameters. We assume a galaxy bias of unity.

Table 2. Ratios of dark energy figures of merit, Gaussian to non-Gaussian

Survey	$k_{\text{max}} [h \text{ Mpc}^{-1}]$		
	0.1	0.2	0.5
Continuous	1.21	1.68	4.72
Sloan Main-type ($\bar{n} = 0.003 h^3 \text{ Mpc}^{-3}$)	1.20	1.59	3.61
BOSS-type ($\bar{n} = 0.0003 h^3 \text{ Mpc}^{-3}$)	1.14	1.28	1.72
Euclid BAO component	1.10	1.27	1.89

Ratio of Dark Energy Task Force figures of merit from Gaussian statistics to those from non-Gaussian. The top three rows refer to the combination of data from three hypothetical 1-Gpc³ surveys (at $z = 0, 0.5, 1$). The first row shows the limiting case of a continuous matter field; the second and third add shot noise roughly equivalent to that in the Sloan MGS ($\bar{n} = 0.003 h^3 \text{ Mpc}^{-3}$) and that in BOSS ($\bar{n} = 0.0003 h^3 \text{ Mpc}^{-3}$). For this table only, we include a galaxy bias of 1.5 for the MGS-type sample and 1.7 for the BOSS-type sample. (Thus the second and third rows do not match the corresponding curves in Fig. 5, which include no bias). See text for details on our modeling of the Euclid BAO component, shown in the fourth row.

figure of merit, defined by Albrecht et al. (2006) as

$$\text{FOM}_{\text{DETf}} = [\det \text{Cov}(w, w_a)]^{-1/2}, \quad (18)$$

where $\text{Cov}(w, w_a)$ indicates the covariance submatrix for w and w_a . To illustrate the impact of galaxy bias (which we have ignored for the majority of this paper) we include the following biases in Table 2 only but *not* in Fig. 5: to more closely simulate the surveys, we assume (in Table 2) a bias of 1.5 for the Sloan-MGS type survey

(Howlett et al. 2015) and a bias of 1.7 for the BOSS-type survey (Gil-Marín et al. 2015). Note once again the significant effect of assuming Gaussianity: for $k_{\text{max}} = 0.5 h \text{ Mpc}^{-1}$ and Sloan-MGS type surveys (assuming a bias of unity), one obtains a figure of merit 2.86 times greater than it should be. Adding the bias makes the results even more dramatic: these calculations show that even a sparse BOSS-type survey would have a figure of merit 72 per cent higher under Gaussian assumptions than under non-Gaussian, and Gaussian assumptions would inflate the figure of merit for an MGS-type survey by 3.6 times.

In connection with this result, note first that our covariance matrix (from which we calculate the figure of merit) employs all the information in the power spectrum rather than considering the peak position only. Second, while galaxy biasing (like shot noise) can reduce the information in the spectrum, comparison of Table 2 with Fig. 5 demonstrates that the magnitude of this effect depends on one’s assumptions about the Gaussianity of the field. Since the bias is degenerate with σ_8 , it is likely that this effect is more pronounced for amplitude-like parameters. A joint analysis with the CMB could help to alleviate this degeneracy.

We emphasize in particular that it is the matter power spectrum which forms the basis for these calculations, and that we simulate galaxies by means of shot noise. Thus it is likely that the behavior of real galaxies will differ to some degree from that presented here.

In this connection, we must also briefly consider the following effect which we have neglected throughout this work: for very sparse samples on very small scales, our shot noise approximation (using $1/\bar{n}$) is no longer accurate; instead, the ratio of con-

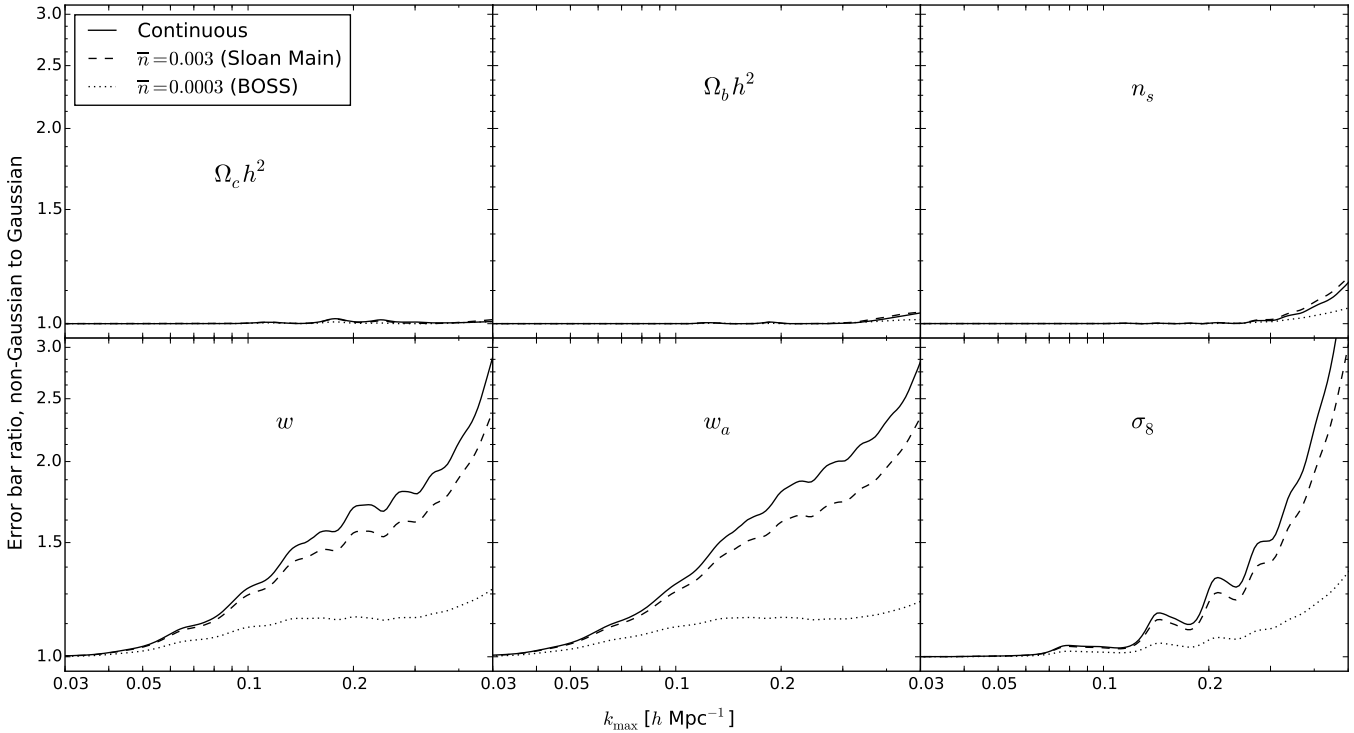


Figure 4. Ratio (non-Gaussian to Gaussian) of the sizes of marginalized error bars for the combined results of three hypothetical 1-Gpc³ surveys at $z = 0, 0.5,$ and 1. Solid lines represent the limiting case of a continuous matter field; dashed and dotted lines assume Poisson sampling with $\bar{n} = 0.003$ and $0.0003 \text{ h}^3 \text{ Mpc}^{-3}$, respectively (comparable to the SDSS MGS and to the BOSS sample). We use Equation 9 to calculate the information for non-Gaussian cases. We assume a galaxy bias of unity.

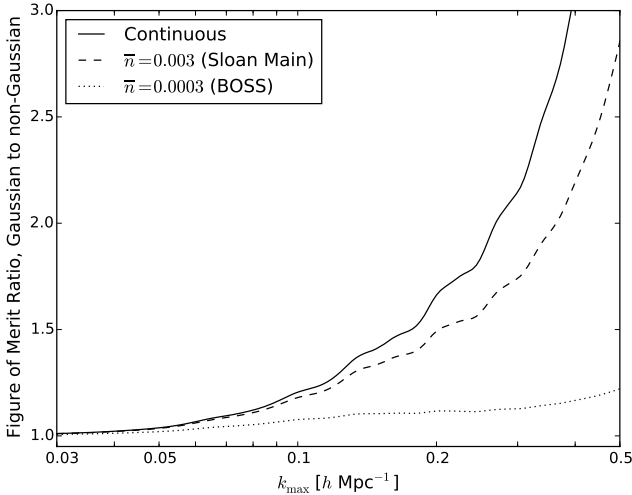


Figure 5. Ratio of the Dark Energy Task Force figure of merit under Gaussian assumptions to that under non-Gaussian assumptions. Calculations assume the combination of three hypothetical 1-Gpc³ surveys at $z = 0, 0.5,$ and 1. The solid curve represents the limiting case of a continuous matter field; the dashed and dotted lines assume Poisson sampling with $\bar{n} = 0.003$ and $0.0003 \text{ h}^3 \text{ Mpc}^{-3}$ (comparable to the SDSS MGS and to the BOSS sample). Note that this figure differs from Table 2 by including no bias for the galaxy-sampling curves.

tributed information per k -mode under Gaussian and non-Gaussian assumptions approaches unity. This effect occurs when there is one galaxy (or fewer) per mode, in which case additional modes

would contribute no additional information. As a result one obtains a freezing of the ratios at such scales. For BOSS-type surveys one reaches this scale around $k = 0.3h \text{ Mpc}^{-1}$; thus for such surveys and for amplitude-like parameters, the information ratio would freeze around 1.1 (or 1.3 including the bias). For Sloan-MGS type surveys, however, the corresponding threshold lies well above $k_{\text{max}} = 0.5h \text{ Mpc}^{-1}$ indicating that the forecasting errors will indeed be as grave as shown in Fig. 4, Fig. 5, and Table 2.

The hypothetical surveys considered so far are artificial in that they assume the same number density and survey volume at $z = 0$ as at $z = 1$. Thus we conclude by analyzing the BAO component of the upcoming Euclid survey², calculating and combining the Fisher information in seven redshift bins ($\Delta z = 0.2$) from $z = 0.65$ to $z = 2.05$. Fig. 3.2 in Laureijs et al. (2011) provides the number of galaxies in each bin, and the survey area of $15,000 \text{ deg}^2$ then yields the volume and average galaxy number density for each. The number densities in the bins range from $\bar{n} = 0.0015 \text{ h}^3 \text{ Mpc}^{-3}$ in the lowest bin to 0.0001 in the highest, peaking at 0.0017 at $z \sim 1$. We include a linear bias $b = 1.5$ (similar to that of the Sloan MGS). And we find (Table 2) that Gaussian assumptions produce a figure of merit (for $k_{\text{max}} = 0.5h \text{ Mpc}^{-1}$) that is almost twice as large as under non-Gaussian assumptions.

We thus conclude that forecasts in the linear regime can assume Gaussian statistics with relative impunity; however, for higher wavenumbers it is essential to account for non-Gaussianity in surveys that seek to constrain amplitude-like parameters in general and dark energy parameters in particular.

² <http://sci.esa.int/euclid/>

7 CONCLUSION

Forecasts of galaxy surveys' effectiveness typically assume a Gaussian field, whereas the actual field is decidedly non-Gaussian. Starting with the CWS15 approximation (Equation 7) for the power spectrum covariance, we have developed a forecasting method which takes into account the non-Gaussianity of the galaxy field. Our method produces results comparable to those obtained from simulations, which is not surprising given the derivation of the CWS15 approximation itself from simulations.

Upon application of our method to hypothetical surveys, we find that the effects of non-Gaussianity are fairly minimal in the linear regime; thus Gaussian-based forecasting is relatively accurate in the regime to which it has heretofore been applied. However, we show that non-Gaussianity can have a profound effect in the non-linear regime. For a galaxy number density of $\bar{n} = 0.003h^3 \text{ Mpc}^{-3}$ (typical of the Sloan Main Galaxy Sample) and at $k_{\text{max}} = 0.5h \text{ Mpc}^{-1}$, Gaussian assumptions can result in significant overestimates of information on all parameters, up to an order of magnitude for w and σ_8 .

However, we find that marginalization also plays a key role in determining which parameters are affected by non-Gaussianity. In particular, marginalization concentrates the effects into amplitude-like parameters such as w , w_a , and σ_8 . We have shown that this behavior is a consequence of the specific form of the covariance matrix. And we proceed to show that error predictions for amplitude-like parameters can be 2.4 times as large as Gaussian forecasting would suggest. Indeed, when we take galaxy bias into account, Gaussian forecasting can produce a dark energy figure of merit well over three times greater than warranted. And for the BAO component of the Euclid survey in particular, we have shown that the assumption of Gaussianity would lead to figures of merit almost twice as optimistic as they should be.

So far we have applied this method to hypothetical galaxy surveys and to Euclid. However, nothing would hinder its application to other surveys (given those surveys' parameters), and for this purpose we make available³ our code implementing this method.

We conclude that in the translinear regime for w , w_a , and σ_8 , accuracy in forecasting depends critically on one's assumptions about the statistics of the underlying field, and that the assumption of Gaussianity can lead to profoundly erroneous forecasts.

This sensitivity to non-Gaussianity is a consequence of a fundamental limitation of the usual δ -based power spectrum, namely, that the information content saturates at high k -values, rendering the remaining information inaccessible. Rimes & Hamilton (2005) and Neyrinck et al. (2006) note that consideration of higher-order statistics does not alleviate this problem, a fact which Wolk et al. (2013) confirmed empirically with Canada-France-Hawaii Telescope Legacy Survey (CFHTLS) data.

Neyrinck et al. (2009) demonstrate that a logarithmic transformation mitigates this issue. Carron & Szapudi (2013, 2014) rederive and then refine this result, obtaining the alternate "sufficient statistics" observable A^* , which circumvents the information plateau by transforming away the non-Gaussian effects. Wolk et al. (2015b) show that the use of A^* can increase the constraints on cosmological parameters by up to a factor of two, and Wolk et al. (2015a) provide an analytic framework for A^* -based forecasting. In addition, Wolk et al. (2015) show that the combination of A^* with the CWS15 covariance matrix (Equation 7) can improve constraints on neutrino masses by almost a factor of three, compared

to using the matter power spectrum. Thus, non-Gaussianity will have a profound impact on forecasts of future surveys, if those forecasts use the traditional δ power spectrum. However, an alternate statistic for obtaining accurate forecasts is already available.

IS, JC, and MW acknowledge NASA grants NNX12AF83G and NNX10AD53G for support. The research leading to these results has received funding from the European Research Council under the European Union's Seventh Framework Programme (FP/2007-2013) / ERC Grant Agreement No. [616170]. We also thank Mark Neyrinck for his helpful suggestions for improvement of the manuscript.

REFERENCES

- Albrecht A., et al., 2006, (arXiv:astro-ph/0609591)
 Albrecht A., et al., 2009, (arXiv:0901.7021)
 Anderson L., et al., 2012, MNRAS, 427, 3435
 Bardeen J. M., Bond J. R., Kaiser N., Szalay A. S., 1986, ApJ, 304, 15
 Baumgart D. J., Fry J. N., 1991, ApJ, 375, 25
 Bennett C. L., et al., 2013, ApJS, 208, 20
 Blake C., et al., 2011, MNRAS, 418, 1707
 Bond J. R., Efstathiou G., 1987, MNRAS, 226, 655
 Bouchet F. R., Strauss M. A., Davis M., Fisher K. B., Yahil A., Huchra J. P., 1993, ApJ, 417, 36
 Carron J., 2011, ApJ, 738, 86
 Carron J., Neyrinck M. C., 2012, ApJ, 750, 28
 Carron J., Szapudi I., 2013, MNRAS, 434, 2961
 Carron J., Szapudi I., 2014, MNRAS, 439, L11
 Carron J., Wolk M., Szapudi I., 2015, MNRAS, 453, 450
 Cole S., et al., 2005, MNRAS, 362, 505
 Cramér H., 1946, *Mathematical Methods of Statistics*. Princeton UP, Princeton, NJ
 Fisher R. A., 1925, *Proceedings of the Cambridge Philosophical Society*, 22, 700
 Fry J. N., 1984, ApJ, 279, 499
 Fry J. N., Peebles P. J. E., 1978, ApJ, 221, 19
 Gaztanaga E., 1994, MNRAS, 268, 913
 Gil-Marín H., Noreña J., Verde L., Percival W. J., Wagner C., Manera M., Schneider D. P., 2015, MNRAS, 451, 539
 Hamilton A. J. S., Rimes C. D., Scoccimarro R., 2006, MNRAS, 371, 1188
 Hearin A. P., Zentner A. R., Ma Z., 2012, *J. Cosmology Astropart. Phys.*, 4, 34
 Heitmann K., Higdon D., White M., Habib S., Williams B. J., Lawrence E., Wagner C., 2009, ApJ, 705, 156
 Heitmann K., White M., Wagner C., Habib S., Higdon D., 2010, ApJ, 715, 104
 Howlett C., Ross A. J., Samushia L., Percival W. J., Manera M., 2015, MNRAS, 449, 848
 Hu W., Haiman Z., 2003, *Phys. Rev. D*, 68, 063004
 Jungman G., Kamionkowski M., Kosowsky A., Spergel D. N., 1996a, *Phys. Rev. D*, 54, 1332
 Jungman G., Kamionkowski M., Kosowsky A., Spergel D. N., 1996b, *Physical Review Letters*, 76, 1007
 Laureijs R., et al., 2011, (arXiv:1110.3193)
 Lawrence E., Heitmann K., White M., Higdon D., Wagner C., Habib S., Williams B., 2010, ApJ, 713, 1322
 Lee J., Pen U.-L., 2008, ApJ, 686, L1
 Lewis A., Challinor A., Lasenby A., 2000, ApJ, 538, 473

³ <https://github.com/AREpp/Fisher>

Martínez V. J., 2009, in Martínez V. J., Saar E., Martínez-González E., Pons-Bordería M.-J., eds, *Data Analysis in Cosmology* Vol. 665 of *Lecture Notes in Physics*, Berlin Springer Verlag, *The Large-Scale Structure in the Universe: From Power Laws to Acoustic Peaks*, pp 269–289

Meiksin A., White M., 1999, *MNRAS*, 308, 1179

Mellier Y., 2012, in *Science from the Next Generation Imaging and Spectroscopic Surveys Euclid: Mapping the Geometry of the Dark Universe*, p. 3

Mohammed I., Seljak U., 2014, *MNRAS*, 445, 3382

Neyrinck M. C., 2011a, *ApJ*, 742, 91

Neyrinck M. C., 2011b, *ApJ*, 736, 8

Neyrinck M. C., Szapudi I., Rimes C. D., 2006, *MNRAS*, 370, L66

Neyrinck M. C., Szapudi I., Szalay A. S., 2009, *ApJ*, 698, L90

Neyrinck M. C., Szapudi I., Szalay A. S., 2011, *ApJ*, 731, 116

Peebles P. J. E., 1980, *The large-scale structure of the universe*

Planck Collaboration et al., 2014, *A&A*, 571, A1

Planck Collaboration et al., 2015, (arXiv:1502.01589)

Rao C. R., 1945, *Bulletin of the Calcutta Mathematical Society*, 37, 81

Rimes C. D., Hamilton A. J. S., 2005, *MNRAS*, 360, L82

Sefusatti E., Crocce M., Pueblas S., Scoccimarro R., 2006, *Phys. Rev. D*, 74, 023522

Seo H.-J., Eisenstein D. J., 2007, *ApJ*, 665, 14

Sharp N. A., Bonometto S. A., Lucchin F., 1984, *A&A*, 130, 79

Smoot G. F., et al., 1992, *ApJ*, 396, L1

Szapudi I., Szalay A. S., Boschan P., 1992, *ApJ*, 390, 350

Takada M., Hu W., 2013, *Phys. Rev. D*, 87, 123504

Takada M., Jain B., 2009, *MNRAS*, 395, 2065

Takahashi R., Sato M., Nishimichi T., Taruya A., Oguri M., 2012, *ApJ*, 761, 152

Tegmark M., 1997, *Physical Review Letters*, 79, 3806

Tegmark M., et al., 2004, *Phys. Rev. D*, 69, 103501

Tegmark M., Taylor A. N., Heavens A. F., 1997, *ApJ*, 480, 22

Vogeley M. S., Szalay A. S., 1996, *ApJ*, 465, 34

Wang Y., et al., 2010, *MNRAS*, 409, 737

Wolk M., Carron J., Szapudi I., 2015a, *MNRAS*, 454, 560

Wolk M., Carron J., Szapudi I., 2015b, *MNRAS*, 451, 1682

Wolk M., McCracken H. J., Colombi S., Fry J. N., Kilbinger M., Hudelot P., Mellier Y., Ilbert O., 2013, *MNRAS*, 435, 2

Wolk M., Szapudi I., Bel J., Carbone C., Carron J., 2015, (arXiv:1504.00069)

APPENDIX A: MARGINALIZATION AND THE NON-LINEAR AMPLITUDE PARAMETER

We here demonstrate that if the non-linear amplitude parameter $\ln A_0$ is one of the parameters under consideration (and if the Fisher matrix is invertible), then non-Gaussianity affects only the covariance of $\ln A_0$. In this derivation, a superscript G denotes a quantity calculated under the assumption of Gaussianity.

We begin with Equation 9:

$$F_{\alpha\beta} = F_{\alpha\beta}^G - \sigma_{\min}^2 \frac{F_{\alpha \ln A_0}^G F_{\ln A_0 \beta}^G}{1 + \sigma_{\min}^2 F_{\ln A_0 \ln A_0}^G}.$$

The Sherman-Morrison formula states that for an invertible square matrix A and vectors u and v ,

$$(A + uv^T)^{-1} = A^{-1} - \frac{A^{-1}uv^T A^{-1}}{1 + v^T A^{-1}u}. \quad (\text{A1})$$

We apply this formula by setting $A = F^G$ and

$$u_\alpha = -v_\alpha = \frac{\sigma_{\min} F_{\ln A_0 \alpha}^G}{\sqrt{1 + \sigma_{\min}^2 F_{\ln A_0 \ln A_0}^G}}. \quad (\text{A2})$$

For notational convenience we assume summation over indices appearing as both super- and subscripts (without thereby implying any contra/covariance). The result is as follows:

$$F_{\alpha\beta}^{-1} = (F^G)_{\alpha\beta}^{-1} + \frac{\sigma_{\min}^2 \left((F^G)_{\alpha\gamma}^{-1} (F^G)_{\gamma \ln A_0} \right) \left((F^G)_{\beta\gamma}^{-1} (F^G)_{\gamma \ln A_0} \right)}{1 + \sigma_{\min}^2 \left(F_{\ln A_0 \ln A_0}^G - (F^G)_{\gamma \ln A_0} (F^G)_{\gamma \delta}^{-1} (F^G)_{\delta \ln A_0} \right)}. \quad (\text{A3})$$

Now if the amplitude parameter $\ln A_0$ is part of the parameter set, then by definition

$$(F^G)_{\alpha\delta}^{-1} (F^G)_{\delta \ln A_0} = \delta_{\alpha \ln A_0}. \quad (\text{A4})$$

It follows that

$$F_{\alpha\beta}^{-1} = (F^G)_{\alpha\beta}^{-1} + \sigma_{\min}^2 \delta_{\alpha \ln A_0} \delta_{\ln A_0 \beta}, \quad (\text{A5})$$

so that the marginalized errors are

$$\sigma_\alpha^2 = \begin{cases} (\sigma_\alpha^G)^2 + \sigma_{\min}^2 & \text{if } \alpha = \ln A_0 \\ (\sigma_\alpha^G)^2 & \text{if } \alpha \neq \ln A_0 \end{cases}, \quad (\text{A6})$$

which was to be proved.